SAND2015-1740C

9th U.S. National Combustion Meeting
Organized by the Central States Section of the Combustion Institute
May 17-20, 2015
Cincinnati, Ohio

One-dimensional turbulence simulation of soot and enthalpy evolution in ethylene jet diffusion flames

John C. Hewson[1,*], *David O. Lignell*[2], *Sean P. Kearney*[3], *Daniel R. Guildenbecher*[3], *Victoria Lansinger*[2]

[1]*Fire Science and Technology Department, Sandia National Laboratories, Albuquerque, NM, 87185-0836, USA*
[2]*Chemical Engineering, Brigham Young University, 350 Clyde Building, Provo, UT 84602, USA*
[3]*Diagnostic Sciences and Engineering Department, Sandia National Laboratories, Albuquerque, NM, 87185-0826, USA*
[*]*Corresponding author, email: jchewso@sandia.gov*

Soot formation modeling in turbulent flames depends on many processes including modeling of the fluid dynamics, combustion chemistry, soot chemistry, soot particle size distribution, the interaction among these, as well as turbulent closure models. Recent results of soot formation in a turbulent jet flame using the one-dimensional turbulence (ODT) model have shown good agreement with direct numerical simulations and measurements. We present ODT simulations of experimental ethylene jet diffusion flames and then study the extended parameter space by varying Damköler numbers. Gas temperature, soot concentrations, and radiative losses are quantified.

1 Introduction

In hydrocarbon flames, a fraction of the carbon is converted to soot within the flame. Most of that soot is oxidized as it is advected into the flame, but a fraction is often emitted. In engineered devices this fraction emitted is small but important because of the significant health hazard posed by fine particles [1]. In fires, longer residence times lead to increased soot production and a significant fraction is emitted as smoke.

Soot is also important in radiation heat transfer. The overlap of soot concentrations with high temperature regions provides a significant source of heat flux in many combustion systems as well as in fires. At the same time, soot that is emitted or advected into cool regions absorbs radiative flux and this smoke shielding reduces the radiant flux.

Soot formation and growth are among the slower important processes in hydrocarbon flames, and quasi-steady state concepts do not apply. For example, a steady-state solution to soot in a counterflow laminar flame does not apply because the mixing rates evolve faster than soot adapts to the changing state. Soot evolution also differs from the evolution of gas-phase species in that soot diffusion is negligible in comparison to gas-phase diffusion. It has been observed that the diffusion of the gas-phase composition, represented by the mixture fraction, past the soot is the significant

term in moving soot between rich and lean regions of the flame. There are two components to this evolution, a mean evolution and fine scale fluctuations about this mean. In the past, these fine scale fluctuations have been represented as a diffusive process based on the rate of mixture fraction fluctuations [2].

Recently, direct numerical simulation (DNS) has been applied to study the evolution of soot early in the flame [3–7]. This work has helped to identify some of the long time scales that are unsteady and the significance of the mixture fraction diffusion. However, the temporal restrictions on these simulations to date have prevented studies of soot evolution through the entire history of the flame, limiting our understanding of the significance of turbulence fluctuations in soot oxidation, and ultimately limiting our understanding of soot emissions. In addition, soot radiation plays a significant role in weakening flames and allowing soot emissions, and DNS has not yet reached time scales sufficient to study these radiative losses.

In this work we apply a stochastic model to represent the evolution of turbulence referred to as the one-dimensional turbulence (ODT) model [8–11]. ODT resolves the full range of spatial scales in a single dimension along with the full range of temporal scales, but it relies on a model for the nonlinear turbulent advection process that is based on a resolved velocity field evolution. Evolving a single dimension allows the simulation of differential diffusion and detailed chemistry for combustion over flame evolution times, and ODT has been used to study processes that depend on both difusive processes and the full resolution of the chemical time scales like extinction and reignition [12, 13] and soot evolution [2, 14]. The combined single spatial dimension with temporal evolution makes ODT suitable for studying parabolic flows like jet flames [15, 16], and it also has been applied to buoyant fire plumes [14].

We describe the evolution of soot in a turbulent jet flame using ODT. The parameter space is selected to result in significant conversion of fuel carbon to soot and significant radiative enthalpy losses. There are modest soot emissions in this flame and the chemistry of soot production is adjusted to vary these emissions. The flame is in a regime where perturbations to the soot loading significantly alter the radiative losses and this plays a role in emissions.

2 Model description

The ODT model is described in detail in the literature [8–11], and only a summary is provided. More detailed information on the ODT code used in this study is given in Ref. [11]. Here, we solve transport equations for mass, momentum, enthalpy, gaseous species mass fractions, and three soot moments. The ODT code uses a Lagrangian finite volume formulation for the diffusive advancement. Automated adaptive mesh refinement (AMR) approach is used. In the Lagrangian formulation, mass is constant inside grid cells and cell volumes expand or contract due to combustion dilatation. This diffusive advancement of the transport equations is punctuated by concurrently occurring eddy events that model turbulent advection. Eddies are sampled randomly on the domain, with a size drawn from a sample distribution (whose form affects only the solution efficiency). A given eddy of size l and location x_0 has an eddy timescale τ and associated eddy rate $1/\tau$, and eddies occur in accordance with their given rates as a Poisson process.

Three ODT parameters govern the eddy event process: the eddy rate parameter C, which scales the rate of occurrence of eddies; the viscous penalty parameter Z, which suppresses small eddies;

and the large eddy suppression parameter β, which constrains eddies such that $t_e \geq \beta\tau$, where t_e is the elapsed time of the simulation.

The gas chemistry is a 19 species 167 reaction reduced mechanism described in [3]. The soot model is detailed in [5]. The soot chemistry is that given by Leung et al. [17], and consists of nucleation, growth, oxidation, and coagulation. The nucleation and growth species is acetylene, and oxidation is written in terms of molecular oxygen. Three soot moments are transported and the moment equations are closed using an assumed lognormal size distribution. Soot and gas reactions are coupled so as to maintain a mass balance due to soot formation or oxidation. Radiative transport is modeled using a grey, two-flux formulation (Schuster-Schwartzchild approximation) [18] with temperature-dependent Plank mean absorption coefficients computed for gaseous CO_2, H_2O, CO, and CH_4 [19]. The soot absorption coefficient is computed as in [14].

3 Simulation Configurations

The configuration studied here is a round nonpremixed turbulent ethylene jet flame. The jet is based on the experiments performed by Zhang et al. [20]. Pure ethylene issues into an air coflow, both at 294.15 K and 1 atm. The jet is piloted with an annular premixed ethylene-air flame with a flow rate corresponding to 2% of the heat release of the main jet. The jet diameter is 3.2 mm and the pilot diameter is 15.2 mm. The Reynolds number of the jet is 20,000, which gives a jet exit velocity of 53.7 m/s assuming a fuel kinematic viscosity of 8.6E-6 m^2/s. The coflow air velocity is 0.6 m/s. The pilot velocity is 6.22 m/s assuming a stoichiometric mixture.

The ODT simulation is a planar, temporally-evolving jet. This ODT configuration has been successfully compared to experimental jet flames in Refs. [15, 16], among others. The jet dimensions and flow velocities were set at those given above. However, initial simulations resulted in excessive flame extinction and the width of the pilot was doubled to compensate.

The ODT parameters used in all simulations were $C = 8$, $Z = 400$, $\beta_{les} = 0.8$. These parameters are the same as those used in [21] in comparing ODT to DNS of planar temporal ethylene jet flames with flame extinction and reignition, and were found to give good results for the flame evolution and scalar dissipation rate profiles. The simulations presented are very similar in configuration to the recent experiments performed at Sandia National Laboratories and soot results here are compared to those experimental measurements described in the next section.

Due to uncertainties in soot formation rates, we perform a series of four simulations with soot nucleation and growth rates divided by factors of 1, 2, 4, and 8. These cases are referred to here as Cases R, R/2, R/4, R/8, respectively. The variation in soot formation rates can also be thought of as a variation in the sooting tendency of the fuel as would be found for a similar flame but with a more or less strongly sooting chemistry. We note here that we have not altered the soot oxidation rates proportionately for the specific reason that we wanted to understand the effects variations in the sooting propensity would have on the evolution.

The timescale based on the jet velocity and diameter, d_{jet}/u_{jet}, is 0.06 ms, and the simulations were run for 0.2 s. Simulation times are converted to downstream axial location by transforming time and space using an axially-varying average velocity computed as the ratio of the integrated axial momentum flux to integrated mass flux over the domain [15]. In a fully three-dimensional flow,

there is some difference in the residence time for the central jet and for the near-stoichiometric regions with lower flow velocities. This can be accounted for in the spatially-evolving ODT formulation, but we have not done so here.

4 Experimental Measurements

Measurements of the given flame configuration [20] are available in [22], and recently we have performed additional measurements. Temperature, oxygen and soot measurements were acquired using laser diagnostics. The femtosecond/picosecond coherent anti-Stokes Raman scattering (CARS) scheme described previously [23, 24] was used for joint temperature/oxygen measurements on a single-laser-shot basis at 1-kHz data rate. The CARS measurement volume for these point measurements was well-approximated by an ellipsoid with 50 μm minor-axis and 1.5 mm major-axis diameters. Measurements in the product gases of premixed ethylene/air flat flames on the McKenna burner were used to access the accuracy of the temperature measurements at 3% with a precision of 1-2% [24]. Similarly, the accuracy and precision of measured O_2/N_2 mole-fraction ratio were 5-10% and 1-2%, respectively, for O_2/N_2 values of 6-20%. Below O_2/N_2 = 6%, measurement uncertainty degrades as the detection limit for oxygen of O_2/N_2 $\sim$1-2% is approached. At low (T $<$ 1000 K) temperatures and oxygen content in excess of O_2/N_2 = 20%, the oxygen sensitivity in the present measurements appeared to degrade as well. Measured CARS spectra were fit to the phenomenological model described in [24]. A threshold on the goodness-of-fit parameter was used to discard $\sim$25% of spectra that did not yield quality model fits.

Single-laser-shot soot measurements were obtained at 10 Hz in a 2-D measurement plane near the radial center of the jet flame using planar laser-induced incandescence. Calibration of the LII signal was performed against light-extinction measurements using the method described in [25]. The LII field of view was 34-mm x 34-mm, with an in-plane resolution of $\sim$60 μm. The out-of-plane resolution was dictated by the thickness of the 1064-nm Nd:YAG laser sheet, which varied in the horizontal dimension from 100-200 μm near r/D = 0 to $\sim$400-500 μm near the lateral edges of the field of view. LII was collected in the plateau-level regime [26], with a high laser fluence of 3.5 J/cm^2, to minimize the impact of varying laser-sheet thickness on the LII soot calibration. Soot probability densities were constructed for comparison to ODT model predictions by considering the data at each pixel as a single point measurement, and binning the results from all pixels acquired over 500 single-laser-shot realizations to build histograms of soot volume fraction. Four independent soot pdf results were constructed with the LII field of view centered at z/D = 77, 87, 97, and 107. A preliminary estimate of the accuracy and precision in our single-shot soot f_v data of 22% and 15-30%, respectively, was obtained based on previous LII work in our laboratory [25]. This estimate neglects absorption of the LII signal by soot at this stage.

5 Results

The overall ODT flame evolution is depicted by the temperature field in Fig. 1 for the four cases considered; the mean stoichiometric contour line is also shown. In comparing this with measurements for the full flame of the similar configuration reported in Ref. [22] it is possible that the ODT prediction is slightly longer than the actual flame. A contour plot for the average soot mass fraction is shown in Fig. 2 and the effect of the different soot formation rates is clear. In the tem-

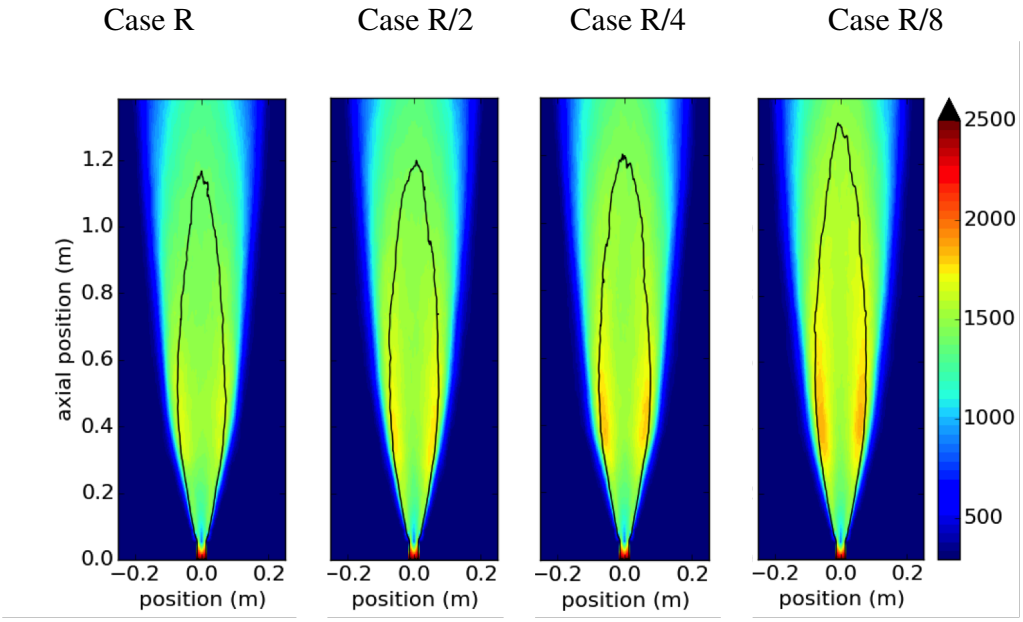

Figure 1: Mean temperature contours for four cases.

perature contour plots differences in the temperature profile are also evident due to soot radiation; the flames with less soot formation exhibit higher temperatures. The flame is slightly longer when less soot is produced; flame length is affected by three factors we have not separately quantified (a) more dilatation due to less radiative losses, (b) less soot formed and emitted requiring more oxygen to oxidize the carbon and (c) greater viscous dissipation suppressing some turbulent mixing.

In Fig. 3 we provide a scatter plot along with conditional averages showing the CARS measurements (with uncertainties projected on the conditional average) together with the ODT predictions for Case R/8 at a height of $x/d = 175$, slightly over half of the flame height. In general results are in good agreement except at very low oxygen and temperature levels where uncertainties are higher. We note that ODT predictions in Case R lead to substantially higher radiative emissions, and the ODT temperature predictions for Case R are well below the measured values plus measurement uncertainty.

LII measurements described above have also been conducted. Average soot volume fractions and PDFs of the soot volume fraction have been determined at four heights. These are compared with ODT predictions for Case R/8 in Fig. 4. For Case R/8 the ODT predictions are in good agreement regarding the average soot volume fraction, the most important quantity for predicting soot emissions. The ODT predictions show a PDF with a peak at slightly larger values suggesting greater intermittency. It is difficult to determine the reasons for this at the present, but the ODT predictions with larger soot rates, Case R for example, predict significantly greater soot concentrations as shown below.

Given the relatively good agreement of the temperature and soot with the measurements for the R/8 production rates, we suggest that this provides the best description of the actual ethene jet flame described in [20]. It is not clear whether the original rates, R, that were derived for ethene flames

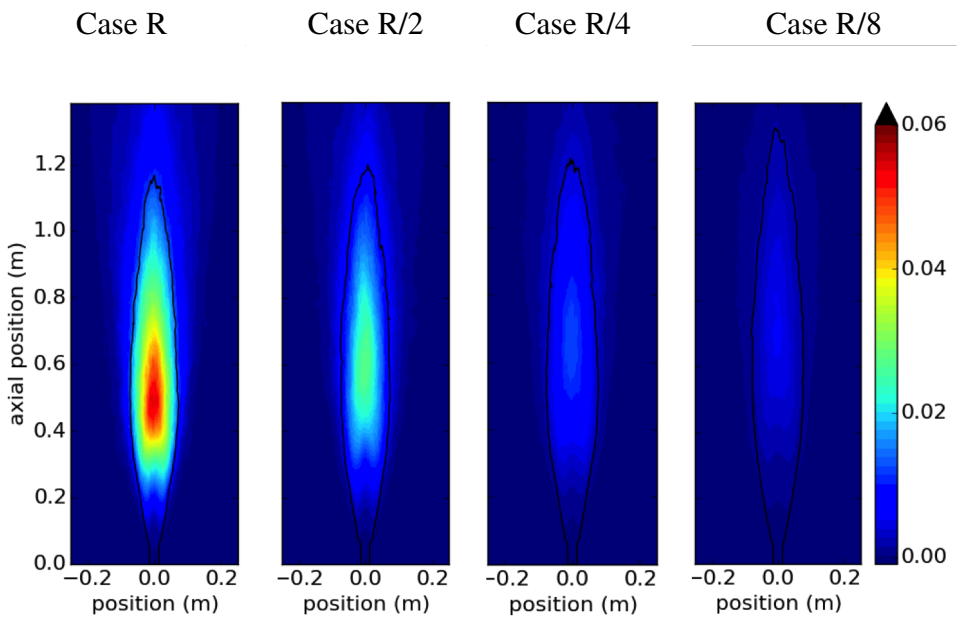

Figure 2: Mean soot mass fraction contours for four cases.

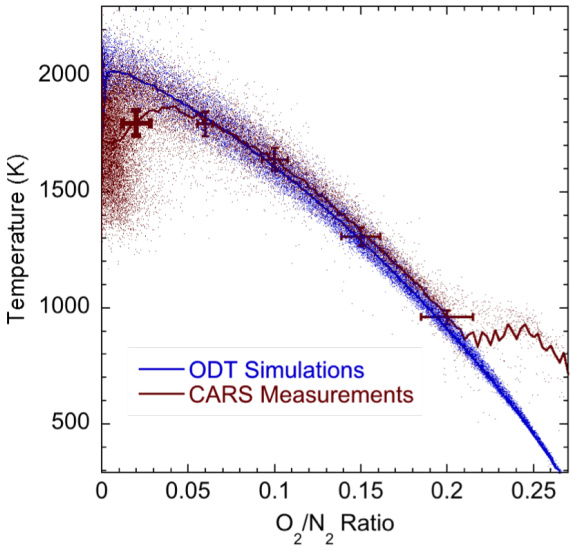

Figure 3: Scatter plots and conditional averages for CARS measurements compared with ODT predictions (Case R/8) for the temperature and O_2/N_2 mole ratio at $x/d = 175$. CARS measurements are taken from the flame center to $r/d = 9.4$ while ODT results are sampled from the full cross-stream region, but there is little radial variation observed in either measurements or predictions.

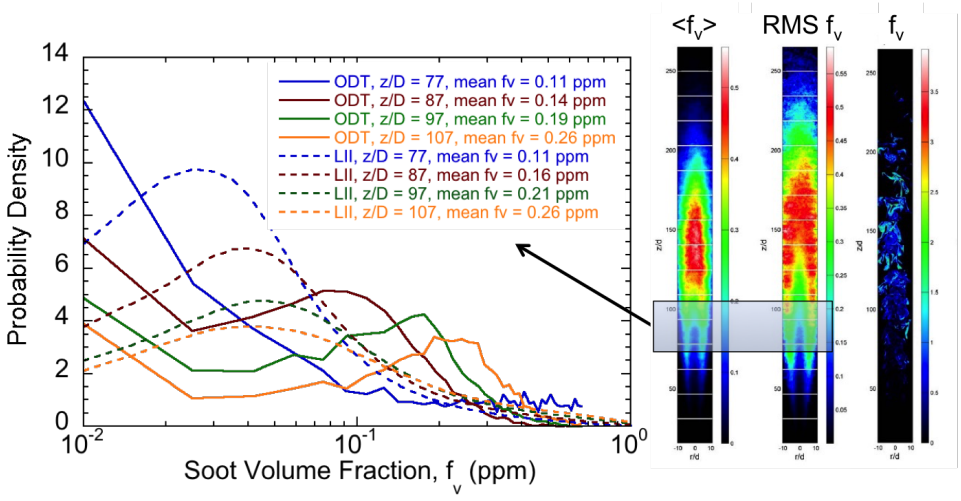

Figure 4: Soot probability density functions for LII measurements compared with ODT predictions for Case R/8 in the region $x/D = 75$ to 110. Average values are indicated in the legend. Images at right from [22].

under a variety of conditions [17] would be suitable for describing this flame under a different set of ODT mixing conditions or whether the rates themselves need to be adjusted for these particular turbulent flames; that is, it is unclear whether the differences are associated with the turbulence model or with the chemistry model. In recent work comparing ODT prediction to DNS, both using this same chemistry and soot model, agreement was good, but the mapping between the temporal DNS and the spatial jet is a potential issue.

As indicated above, a series of four cases is reported with the soot-production rates (nucleation and mass growth rates) differing by a factor of two between each, for a total variation in the soot-production rate of a factor of eight. In Figs. 5 and 6 conditional averages (Favre averages conditional on the value of the mixture fraction) are plotted for these four production rates and at locations that are very approximately 1/4, 1/2, 3/4 and 1 times the flame height to show the evolution.

In Fig. 5 the logarithm of the conditional soot volume fraction is shown. Conditional averages peak in the vicinity of a mixture fraction of 0.15 compared to the stoichiometric value of 0.064. For a given conditional value of the mixture fraction, the soot volume fraction increases as the flow evolves downstream as expected, though this is difficult to see in the logarithmic scale. Values are plotted on the logarithmic scale because a factor of two separation would result with linear sensitivity, and this is observed over parts of the flame. In particular, for the lower rates (R/4 and R/8) in the rich regions ($Z > Z_{st}$) where the enthalpy losses are not too great. When enthalpy losses are significant (see Fig. 6) the soot reaction rates are reduced as will be indicated below. Thus, for the higher soot rates (i.e., Case R) the conditional soot is not twice the next lower rate, especially higher in the flame where radiant losses are more significant.

It is also interesting to note the soot levels to the lean side of the flame, mixture fractions below 0.064. On the lean side the soot levels are substantially reduced, but cases with larger production rates have disproportionately larger levels on the lean side. Rather than being separated by a factor

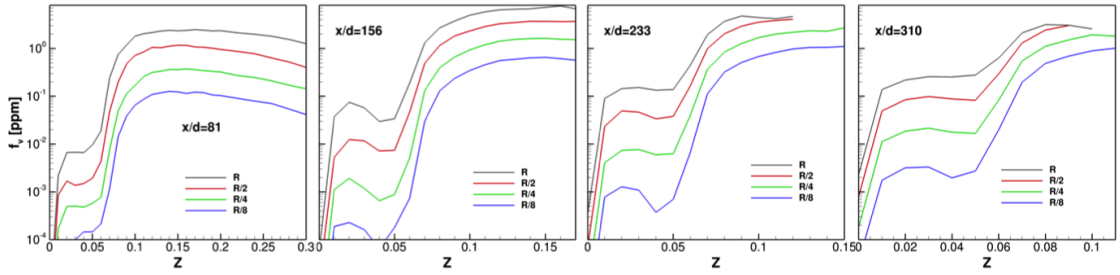

Figure 5: Conditional averages for soot volume fraction at four downstream locations and for four cases.

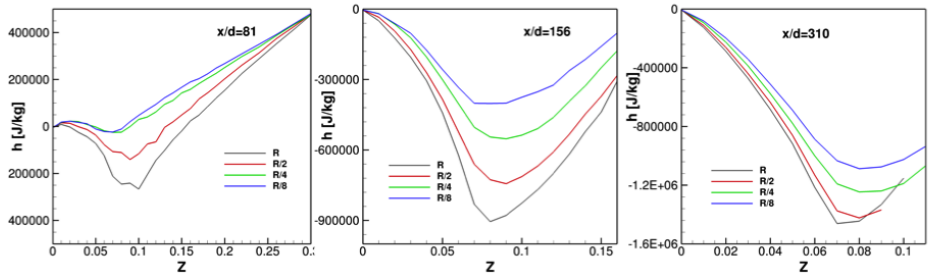

Figure 6: Conditional averages for enthalpy at three downstream locations and for four cases.

of two, the separation is closer to a factor of five, with a factor of 110 between Case R and Case R/8 (the cube root of that being $4.8 \approx 5$) at three-quarters of the flame height.

We also note that conditional fluctuations (not shown here) are large, of the same magnitude as the conditional means, as has been observed previously [2, 14]. This is related to the intermittent nature of soot.

The increased soot levels lead to increased radiant emissions that affect both the temperature and the enthalpy, shown in Fig. 6. The initial enthalpy profile is close to linear with respect to mixture fraction with the fuel enthalpy being about 1.8E6 J/kg. Enthalpy loss due to radiation is evident in all profiles including those as low as one-quarter of the flame height ($x/d = 81$) where soot levels are still well below their peak values. Interestingly, by the top of the flame (near $x/d = 310$), the enthalpy loss by each of the soot rates is of the same approximate magnitude. However, with larger soot-production rates, the losses occur earlier in Cases R and R/2 as seen at heights $x/d = 81$ and 156.

To better visualize the soot and enthalpy evolution through the flame, we present here line integrated quantities. These are the integral of various density-weighted quantities (soot, total carbon, enthalpy) along the ODT line; for example, the line-integrated soot is $\int_{-\infty}^{\infty} \rho Y_s dx$, with units of kg m^{-2} with the area dimension relating to the notional area of the ODT line. In Fig. 7 this quantity is plotted as a function of the height. For reference, the total line-integrated carbon on the ODT domain is 3.4E-02 kg m^{-2} so that the greatest soot levels (maximum for Case R) represent

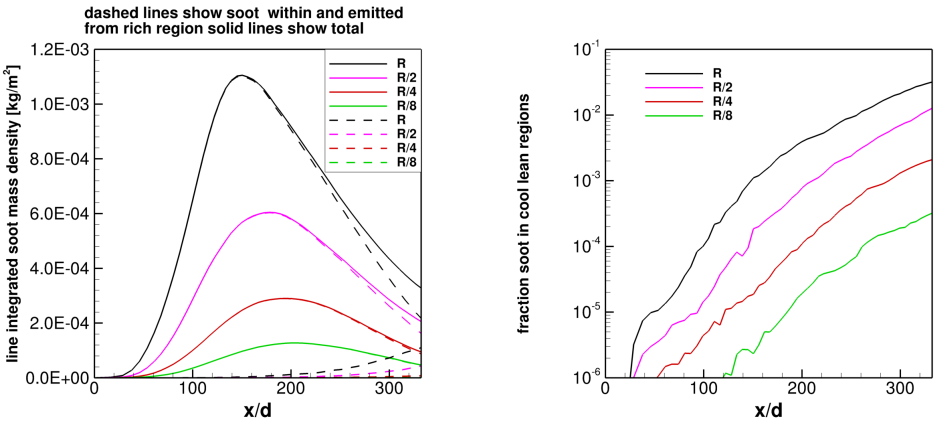

Figure 7: The line integrated masses of soot is plotted (solid) together with dashed lines indicating the soot mass within the flame and emitted is plotted in the left panel. Here, the emitted soot is indicated by the combined condition that $Z < Z_{st}$ and $T < 1400$ K. The right panel shows the carbon in the emitted soot normalized by the total carbon.

approximately one-third of the total carbon in the form of soot.

In addition to the total soot across the domain, we have separated the soot into soot we refer to as 'in cool lean regions,' this is soot that satisfies both $Z < 0.9Z_{st}$ and $T < 1400$ K and is less likely to be oxidized, and the remainder that is 'within the flame' and has a reasonable chance of oxidation. The line-integrated soot in the lean cool regions as well as that within the flame are also plotted in the left panel of Fig. 7 where it can be seen that the vast majority of soot can be taken to be 'within the flame' except as the end of the flame is reached (for the given conditions).

In the right panel of Fig. 7 we plot the soot in the lean cool regions normalized by the total carbon on a logarithmic scale. As in Fig. 5, it is clear in Fig. 7 that increasing the rates by a factor of two leads to emissions that increase by more than a factor of two. The soot in the lean cool regions is separated, on average, by a factor of five, though this is closer to a factor of six difference between Cases R/8 and R/4 and between R/4 and R/2, but only a factor of three difference between Cases R/2 and R. This is the same separation observed by looking at conditional averages in Fig. 5. The reduced separation between the emissions in Cases R/2 and R occurs because that flame cools rapidly enough to reduce soot formation rates before the other cases.

We provide the line-integrated enthalpy deficit in Fig. 8: $\int_{-\infty}^{\infty} \rho[h - H_{ad}(Z)]dx$, with h being the predicted enthalpy and $H_{ad}(Z)$ being the linear (in mixture fraction) interpolation between the air and fuel enthalpies. Figure 8 confirms the previous observation around Fig. 6 that the final enthalpy losses are comparable for the different cases, at least relative to the total enthalpy lost, and that the higher soot rates lead to earlier reductions of enthalpy but that the trajectory is not dramatically different, just shifted in flame position.

In the right panel of Fig. 8 we combine the left panel enthalpy and the fraction of the soot mass in the cool lean regions, plotting the latter as a function of the line-integrated enthalpy. The evolution up through the flame is to the left and up in this figure. There is an interesting correlation in the present results between the soot emissions and the enthalpy deficit. This suggests that the soot

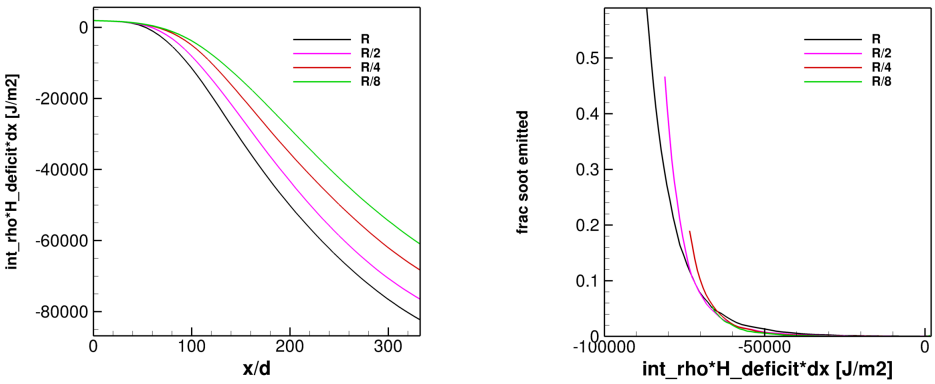

Figure 8: The line integrated enthalpy deficit is plotted in the left panel. In the right panel the fraction of soot emitted normalized by the current soot mass (both line integrated) is plotted as a function of the enthalpy deficit.

emissions rise rapidly once a certain enthalpy deficit is reached. Similar results were found by Ricks et al. [14]. While we expect the magnitude of soot emissions will depend on the mixing rate history, we think that the correlation between the rapid rise in emissions and the enthalpy deficit will be found in other highly sooty flames because this represents the enthalpy where the flame is weakening so that soot oxidation becomes challenging. Further work needs to be done, however, to actually predict emissions in more global terms.

6 Conclusions

We present ODT predictions of an ethylene jet flame including soot growth and oxidation according to a simplified mechanism and including radiation source terms that reduce the enthalpy. ODT predictions are compared with recent measurements of temperature and O_2/N_2 using CARS and soot using LII in a flame of the same configuration.

Simulations are presented over a range of soot-production rates with significant differences in the evolution of the soot mass fractions, the enthalpy and the soot emissions resulting from the different soot-production rates. Until the radiative enthalpy losses get very large, the rich side soot evolution is roughly proportional to the soot-production rates that are varied. On the lean side, however, the interplay of the greater soot levels and the greater enthalpy losses reducing soot oxidation rates leads to soot emissions that are greater than the difference in the production rates. For a factor of two difference in the production rates, the soot emissions are between a factor of three and a factor of six greater.

Acknowledgments

This material is based in part upon work supported in part by the National Science Foundation under Grant No. CBET-1403403 and supported by the Department of Energy National Nuclear Security Agency's Engineering Campaigns Program at Sandia National Laboratories. Sandia Na-

tional Laboratories is a multi-program laboratory managed and operated by Sandia Corporation, a wholly owned subsidiary of Lockheed Martin Corporation, for the U.S. Department of Energy's National Nuclear Security Administration under contract DE-AC04-94AL85000.

References

[1] U.S. Environmental Protection Agency, Air quality criteria for particulate matter, EPA/600/P-99/002aF, October 2004.

[2] D. O. Lignell, G. C. Fredline, and A. D. Lewis. *Proceedings of the Combustion Institute*, 35 (2015) 1199–1206.

[3] D. O. Lignell and J. H. Chen. Direct numerical simulation of soot formation in a three-dimensional nonpremixed ethylene jet flame. In D. Roekaerts, P. Coelho, B. J. Boersma, and K. Claramunt, editors, *Computational Combustion, ECCOMAS Thematic Conference, Delft, The Netherlands*, 2007.

[4] D. O. Lignell, J. H. Chen, P. J. Smith, T. Lu, and C. K. Law. *Combustion and Flame*, 151 (2007) 2–28.

[5] D. O. Lignell, J. H. Chen, and P. J. Smith. *Combustion and Flame*, 155 (2008) 316–333.

[6] D. O. Lignell, J. C. Hewson, and J. H. Chen. *Proceedings of the Combustion Institute*, 31 (2009) 1491–1498.

[7] F. Bisetti, G. Blanquart, M.E. Mueller, and H. Pitsch. *Combustion and Flame*, 159 (2012) 317–335.

[8] A. R. Kerstein. *Journal of Fluid Mechanics*, 392 (1999) 277–334.

[9] A. R. Kerstein, W. T. Ashurst, S. Wunsch, and V. Nilsen. *Journal of Fluid Mechanics*, 447 (2001) 85–109.

[10] W. T. Ashurst and A. R. Kerstein. *Physics of Fluids*, 17-025107 (2005) 1–26.

[11] D. O. Lignell, A. R. Kerstein, G. Sun, and E. I. Monson. *Theoretical and Computational Fluid Dynamics*, (2012) journal.

[12] J. C. Hewson and A. R. Kerstein. *Combustion Science and Technology*, 174 (2002) 35–66.

[13] B. Ranganath and T. Echekki. *Combustion and Flame*, 154 (2008) 23–46.

[14] A. J. Ricks, J. C. Hewson, A. R. Kerstein, J. P. Gore, S. R. Tieszen, and W. T. Ashurst. *Combustion Science and Technology*, 182 (2010) 60–101.

[15] J. C. Hewson and A. R. Kerstein. *Combustion Theory and Modelling*, 5 (2001) 669–697.

[16] T. Echekki, A. R. Kerstein, and T. D. Dreeben. *Combustion and Flame*, 125 (2001) 1083–1105.

[17] K. M. Leung and R. P. Lindstedt. *Combustion and Flame*, 87 (1991) 289–305.

[18] Michael F. Modest. *Radiative Heat Transfer*. McGraw-Hill, New York, 1993.

[19] Y. Ju, H. Guo, K. Maruta, and F. Liu. *Journal of Fluid Mechanics*, 342 (1997) 315–334.

[20] J. Zhang, C. R. Shaddix, and R. W. Shefer. *Review of Scientific Instruments*, 82 (2011) 074101.

[21] D. O. Lignell and D. Rappleye. *Combustion and Flame*, 159 (2012) 2930–2943.

[22] C. R. Shaddix, J. Zhang, R. W. Schefer, J. Doom, J. C. Oefelein, S. Kook, L. M. Pickett, , and H. Wang. Understanding and predicting soot generation in turbulent non-premixed jet flames. Technical Report SAND2010-7178, Sandia National Laboratories, 2010.

[23] S. P. Kearney and D. J. Scoglietti. *Opt. Lett.*, 38 (2013) 833–835.

[24] S. P. Kearney. *Combust. Flame*, (in press, 2014) .

[25] K. Frederickson, S. P. Kearney, and T. W. Grasser. *Appl. Opt.*, 50 (2011) A49–A59.

[26] R. J. Santoro and C. R. Shaddix. Laser-induced incandescence. In K. K. Hoinghaus and J. B. Jeffries, editors, *Applied Combustion Diagnostics*, pages 252–286. Taylor and Francis, 2002.